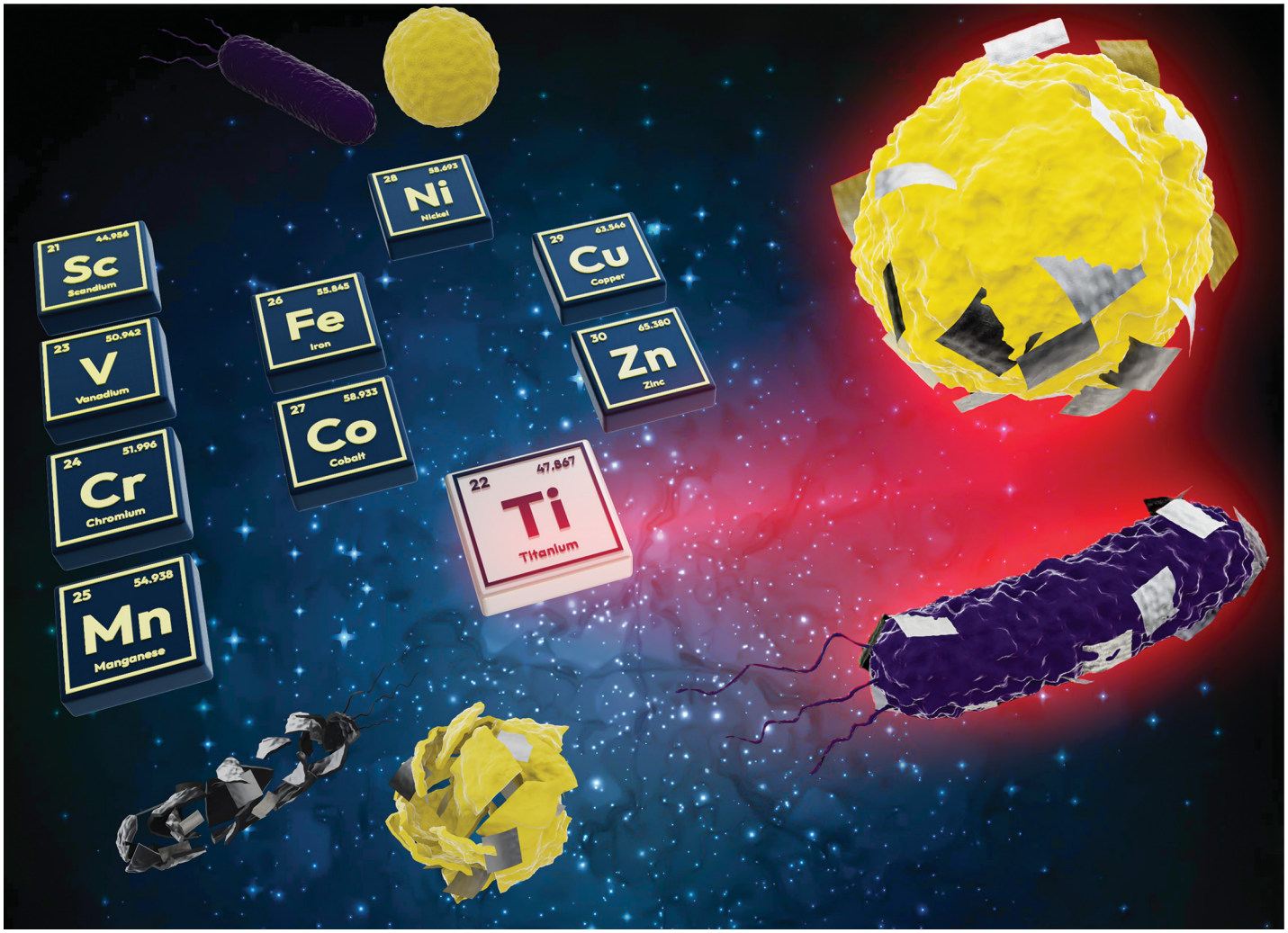

Showcasing research from Anhui Province Key Laboratory of Oral Diseases Research, College and Hospital of Stomatology, Anhui Medical University.

Two-dimensional TiO nanosheets with photothermal effects for wound sterilization

With their excellent mechanical and photothermal bactericidal properties, TiO nanosheets were used as photothermal agents, the only reported use of titanium monoxide in wound healing to date.

As featured in:

See Xianwen Wang *et al.*, *J. Mater. Chem. B*, 2023, **11**, 7641.

ROYAL SOCIETY OF CHEMISTRY

rsc.li/materials-b

Registered charity number: 207890

Journal of Materials Chemistry B

ROYAL SOCIETY OF CHEMISTRY

PAPER

View Article Online
View Journal | View Issue

Cite this: J. Mater. Chem. B, 2023, 11, 7641

Two-dimensional TiO nanosheets with photothermal effects for wound sterilization†

Wei Zhang,‡[a] Hongrang Chen,‡[b] Haotian Tian,‡[c] Qiang Niu,[d] Jianghao Xing,[d] Tao Wang,[e] Xulin Chen[f] and Xianwen Wang *[ad]

Received 23rd May 2023,
Accepted 16th July 2023

DOI: 10.1039/d3tb01170d

rsc.li/materials-b

To combat multidrug-resistant bacteria, researchers have poured into the development and design of antimicrobial agents. Here, low-cost two-dimensional (2D) antibacterial material titanium monoxide nanosheets (TiO NSs) were prepared by an ultrasonic-assisted liquid-phase exfoliation method. When cultured with bacteria, TiO NSs showed intrinsic antimicrobial capacity, possibly due to membrane damage caused by the sharp edges of TiO NSs. Under near-infrared (NIR) laser irradiation, TiO NSs showed high photothermal conversion efficiency (PTCE) and sterilization efficiency. By combining these two antibacterial mechanisms, TiO NSs exhibited a strong killing effect on Gram-negative Escherichia coli (*E. coli*) and Gram-positive methicillin-resistant Staphylococcus aureus (*MRSA*). Especially after treatment with TiO NSs (150 μg mL^{-1}) +near-infrared (NIR) light irradiation, both bacteria were completely killed. *In vivo* experiments on wound repair of bacterial infection further confirmed its antibacterial effect. In addition, TiO NSs had no obvious toxicity or side effects, so as a kind of broad-spectrum 2D antibacterial nanoagent, TiO NSs have broad application prospects in the field of pathogen infection.

[a] College and Hospital of Stomatology, Anhui Medical University, Key Lab. of Oral Diseases Research of Anhui Province, Hefei 230032, China. E-mail: xianwenwang@ahmu.edu.cn
[b] Department of General Surgery, The First Affiliated Hospital of Anhui Medical University, Hefei, 230032, China
[c] Department of Neurosurgery, The First Affiliated Hospital of Anhui Medical University, Hefei 230032, China
[d] School of Biomedical Engineering, Research and Engineering Center of Biomedical Materials, Anhui Medical University, Hefei, 230032, China
[e] Department of Orthopaedics, The Second Hospital of Anhui Medical University, Hefei 230601, China
[f] Department of Burns, The First Affiliated Hospital of Anhui Medical University, Hefei, 230032, China

† Electronic supplementary information (ESI) available. See DOI: https://doi.org/10.1039/d3tb01170d

‡ These authors contributed equally to this work.

Xianwen Wang

Dr Xianwen Wang obtained his PhD degree under the guidance of Prof. Liang Cheng and Prof. Zhuang Liu in the Institute of Functional Nano & Soft Materials (FUNSOM) at Soochow University in 2021. Then he joined Anhui Medical University as a professor and doctoral supervisor. His current research interest is the development of multifunctional nanomaterials for biomedical applications.

Introduction

Multidrug-resistant bacteria pose a serious threat to food, health, and the environment, especially pathogenic resistant bacteria.[1–5] The problem of resistant bacteria has aroused great interest in the development of new antimicrobial agents.[6] Antimicrobials are generally classified into two categories: organic and inorganic.[7,8] Organic antimicrobials are currently the most widely used antimicrobials, but misuse of organic antimicrobials can lead to the emergence and evolution of drug-resistant bacteria. To make matters worse, many organic antimicrobials have the disadvantages of short life, easy decomposition, and low thermal stability, which limits their use in some cases. Therefore, inorganic antimicrobials are widely studied because of their broad-spectrum and intrinsic bactericidal effects.[9–12] Among many inorganic antibacterial agents, silver,[13,14] copper[15–18] and zinc-containing materials are typical representatives.[19,20] However, under light or high temperatures, silver ions are easily reduced to metallic silver, resulting in sample discoloration. In recent years, metal oxides have been widely used as fungicides in biology and medicine. Zinc oxide,[21] copper oxide, and other nanomaterials have been developed into effective antibacterial materials in different fields.[22] Among inorganic antibacterial agents, inorganic nanomaterials with unique structures and morphologies have attracted much attention. These inorganic nanomaterials all share one common property, sharp edges. Therefore, the mechanism of differential bacteriostatic action differs from that of other antimicrobials and

is mainly attributed to bacterial membrane puncture or cutting bacteria caused by sharp edges during physical contact. Surprisingly, unlike antibiotics, these nanomaterials with sharp structures do not have to worry about pathogen resistance to multidrug resistance due to their physical antimicrobial mechanisms. Sunaina *et al.* designed a mechanical bacteriolytic hydrogel dressing for skin lesions infected with Staphylococcus aureus. Gold nanostars have a spiky topology of up to 120 nm and are used to penetrate bacterial membranes.[23] The ability of graphene nanosheets to cleave the cell membrane of *E. coli*, allowing many phospholipids to leak out of the bacterial membrane, is the first report of a two-dimensional (2D) material against disease-causing bacteria.[24] Since then, many 2D materials with graphene-like structures, such as MXene, Sb_2Se_3, MoS_2, and black phosphorus have been used as antimicrobial agents.[25–29] However, most 2D materials themselves have poor antibacterial properties, and only higher doses and longer reaction times can achieve effective sterilization. Therefore, it is of great significance to develop antibacterial agents with intrinsic antibacterial properties.

The synergy of multiple bacteriostatic mechanisms can reduce the dosage of bacteriostatic agents and reduce the toxic side effects of bacteriostatic agents. Near-infrared lasers have the advantages of good penetration, good remote control, and high site specificity in clinical applications.[30] In addition, bacteria are sensitive to heat, and high-temperature treatment can lead to bacterial inactivation. NIR laser irradiation photothermal therapy (PTT) is an effective method to kill bacteria and has been widely studied in recent years.[31–33] Therefore, it is reasonable to expect that materials with photothermal effects and intrinsic antibacterial properties can not only kill bacteria at high temperatures under near-infrared laser irradiation but also improve antibacterial efficiency through the synergy of two antimicrobial mechanisms.[34] The development of antibacterial agents with photothermal effects and intrinsic antibacterial properties may be an important way to improve sterilization efficiency.[35–37]

Titanium monoxide (TiO) is a metal oxide containing a large number of oxygen and titanium vacancies and is often used in electronic equipment.[38,39] Titanium is abundant on Earth and is more abundant than copper and zinc, so it costs less. Titanium has been widely used in the field of human health care, while the application of titanium monoxide in biomedicine has not been reported thus far.[40–42] With these findings in mind, TiO nanosheets (NSs), a promising photothermal 2D material, were used for wound healing, which is the only report to date on titanium-based oxides in wound healing (Scheme 1). With high NIR light absorption and sharp nanosheet edges, TiO NSs have excellent mechanical and photothermal bactericidal properties. Therefore, TiO NSs as photothermal agents for bacterial infection open the door to the application of TiO NSs in wound healing.

Experimental

Materials

Titanium oxide and *N*-methyl pyrrolidone (NMP) were purchased from Shanghai Aladdin Biochemical Technology Co., Ltd. Deionized water used throughout the whole project was obtained through an ultrapure water machine (STAR, Shanghai Zhiding Water Treatment Equipment Co., Ltd). Tryptone soy broth and agar powder were purchased from Beijing Solarbio Science & Technology Co., Ltd. A BCA protein concentration assay kit was purchased from Shandong Sikejie Biotechnology Co., Ltd.

Characterization

HRTEM images and selected regional electron diffraction patterns were obtained by high-resolution transmission electron microscopy (Thermo Scientific Talos F200X). The structural phase and crystallinity of the TiO NSs were determined by X-ray diffraction (XRD, SmartLab SE, Rigaku, Japan). The composition and valence distribution of the elements were identified by X-ray photoelectron spectroscopy (XPS, Thermo Scientific K-Alpha, USA). The UV-VIS absorption spectrum was measured by a UV-visible spectrophotometer (Thermo Scientific Genesys 50, China). SEM images were obtained by field emission scanning electron microscopy (GeminiSEM 300, Germany). The average optical density (OD) value was determined by a Universal Microplate Spectrophotometer (Synergy2 SLFPTAD, USA).

Synthesis of TiO NSs

TiO NSs were prepared by a simple ultrasonic liquid phase stripping method. TiO powder (300 mg) was dispersed into 20 mL glass bottles containing NMP, and ultrasound was carried out in a water bath for 24 hours. After removing larger particles with low-speed centrifugation, using high-speed centrifugation, the materials were washed with ethanol and water several times. The sediment was collected and freeze-dried in a freeze-dryer for future use.

Photothermal performance evaluation

The temperature changes of the TiO NSs at different concentrations were recorded by a thermal imaging camera under laser irradiation at 808 nm and 2.0 W cm^{-2}. Then, an 808 nm laser was used to irradiate 100 μg mL^{-1} TiO NSs at different power densities for 5 min, and the temperature changes were observed and recorded. Three temperature rise/fall curves of 100 μg mL^{-1} TiO NSs were recorded at 808 nm, 2.0 W cm^{-2}.

In vitro antibacterial assays

MRSA and *E. coli* are typical Gram-positive and Gram-negative bacteria, respectively. First, the plate calculation method was used to evaluate the antibacterial activity of TiO NSs *in vitro*. Briefly, different concentrations of TiO NSs were placed into a 1.5 mL centrifuge tube, and 1 mL of bacteria (1.0×10^7 CFU mL^{-1}) was added to the tube. After incubation at 37 °C for 2 h, the bacteria were irradiated with an 808 nm near-infrared laser (2.0 W cm^{-2}) for 6 min. The remaining viable bacteria were counted on the agar plate. The *in vitro* antibacterial group (including the control group, control + NIR group, and TiO group) was studied by the same method. A BCA protein concentration assay kit was

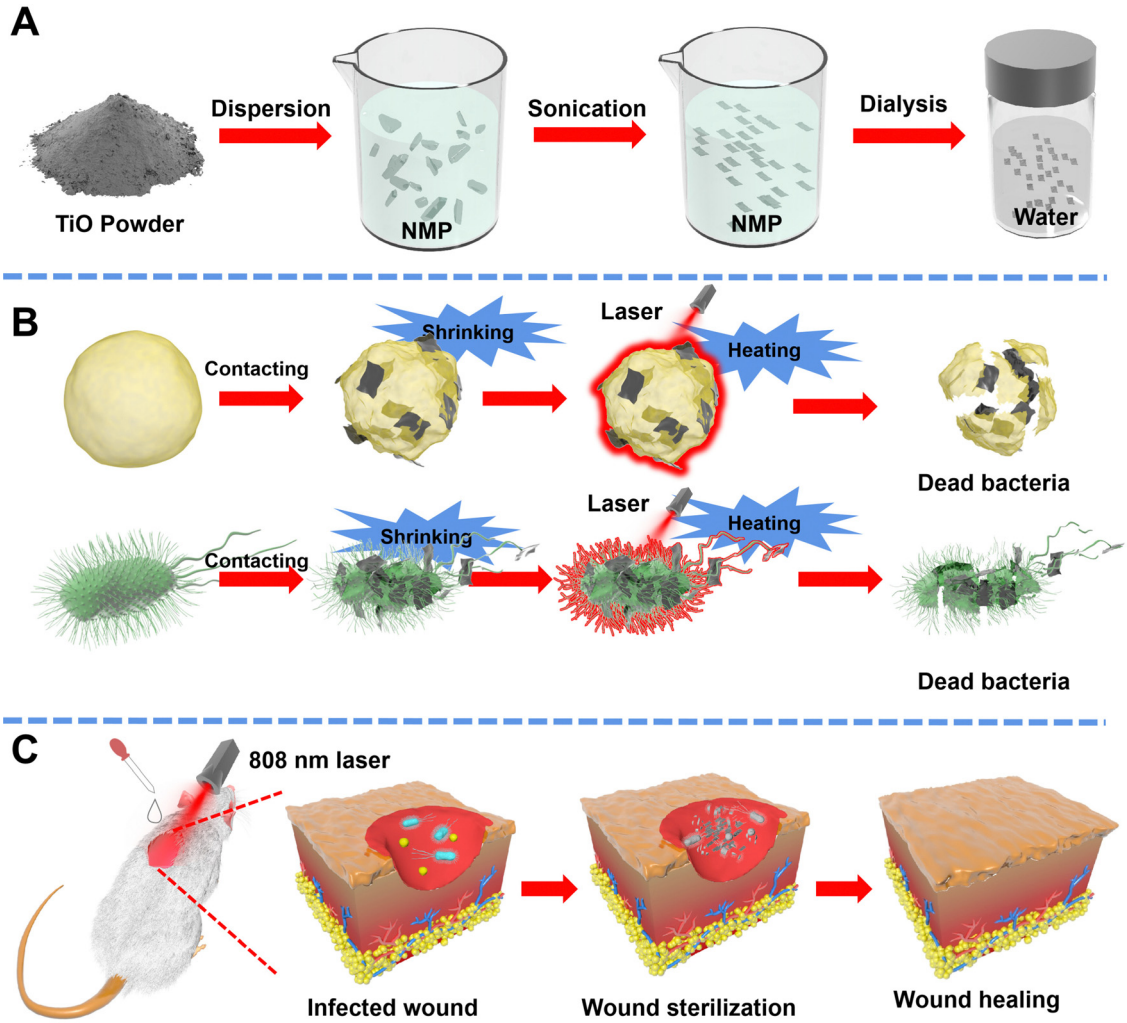

Scheme 1 Schematic illustration of TiO NSs with photothermal effects for wound sterilization. (A) Schematic diagram of the preparation process of TiO NSs. (B) Antibacterial therapy of TiO NSs. (C) Accelerated infected wound healing.

used to detect bacterial protein leakage. Simply, BCA reagent was mixed with Cu reagent at a ratio of 50 : 1 to form a BCA working liquid. One hundred microliters of BSA standard were diluted with PBS to 1 mL so that the final concentration of BSA was 0.5 mg mL^{-1}. Different concentrations of bovine serum albumin were mixed with a BCA working solution and incubated at 37 °C for 15–30 minutes. The absorption value at 562 nm was measured by a spectrophotometer, and the standard curve was drawn. The protein concentration was calculated according to the standard curve. For morphological analysis, the bacteria were collected by centrifugation, fixed with 2.5% glutaraldehyde, and incubated at 4 °C for 12 h, and the glutaraldehyde was removed by bacterial centrifugation. The bacteria were treated with a series of ethanol (30, 50, 70, 80, 90, 95, and 100%) for 10 minutes. The morphology of the bacteria was observed by field emission scanning electron microscopy. In addition, the viability of bacteria was studied by directly observing live and dead bacteria. Briefly, 300 μL of bacterial suspension (1×10^7 CFU mL^{-1}) in different groups was darkened for 30 minutes with a double fluorescent dye containing SYTO 9 and propidium iodide. The bacterial solution was then rinsed with sterile water, placed on a slide, and observed with confocal laser scanning microscopy (CLSM).

In vivo antibacterial experiments

Mice were anesthetized with 1% pentobarbital sodium at a dose of 30 mg kg^{-1}. Create a circular wound approximately 9 mm in size on each rat's back. Then, 100 μL Staphylococcus aureus (1×10^7 CFU mL^{-1}) was injected into the wound and incubated for 10 h to obtain the wound infection model of mice. Mice were randomly divided into the control group, NIR group, TiO group, and TiO + NIR group and were given different treatments ± NIR spectra. Under a near-infrared laser (808 nm, 1.0 W cm^{-2}) irradiation or no irradiation, the wound was photographed every day, and the area of the wound was measured by ImageJ software. After 7 days of treatment, all mice were killed painlessly, and the infected wounds were collected and treated with 10% paraformaldehyde, embedded in paraffin, and sliced. The effect of TiO NSs on wound healing

was observed after staining with hematoxylin and eosin (H&E) and Masson staining. In addition, to further determine the biosafety of TiO NSs *in vivo*, the major organs (heart, liver, spleen, lung, kidney) of TiO NSs-treated and untreated mice were collected for H&E staining analysis. Blood samples were collected from TiO NSs-treated and untreated mice for routine blood tests and biochemical examinations. All animal experiments were conducted by the Committee for Animal Protection and Utilization of Anhui Medical University (No. LLSC20220731).

Results and discussion

TiO NSs were prepared by a liquid ultrasonic exfoliation process. High-resolution transmission electron microscopy (HRTEM) in Fig. 1A–D shows that the TiO NSs had a typical flake morphology and transverse size of 100–200 nm. The size of the TiO NSs was measured using dynamic laser light scattering. The average hydrodynamic diameter of the CNPs was 143 nm (Fig. S1, ESI†). According to high-resolution TEM (Fig. 1E), the lattice spacing was 0.38 nm, consistent with the

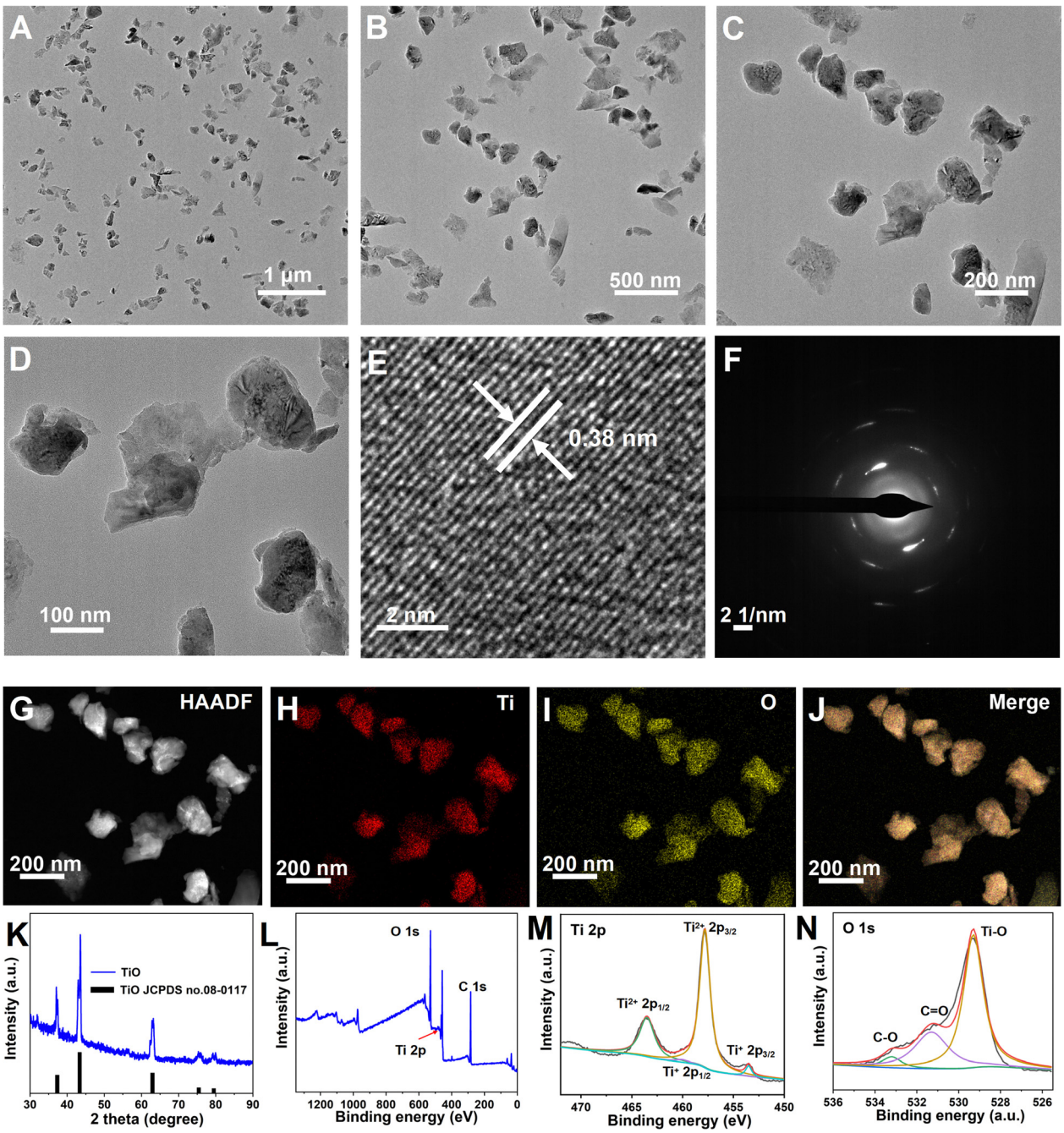

Fig. 1 Characterization of TiO NSs. (A)–(D) TEM images of TiO NSs. (E) HRTEM image of TiO NSs. (F) Selected area diffraction pattern of TiO NSs. (G)–(J) STEM-EDS mapping. (K) XRD spectra of TiO. (L)–(N) XPS spectra of TiO.

crystal plane spacing of (311). The uniform distribution of Ti and O elements was confirmed by scanning transmission electron microscopy (STEM) mapping images (Fig. 1G–J). From Fig. 1K, the peaks in the X-ray diffraction pattern of the prepared material correspond to those of the standard card. From Fig. 1M, the characteristic peaks of the $Ti^{+}2p_{1/2}$ and $Ti^{+}2p_{3/2}$ orbitals appear at binding energies of 460.18 eV and 453.48 eV, respectively, which proves the existence of Ti^{+}. From Fig. 1N, the peak at 529.28 eV indicates the presence of Ti–O. X-ray diffraction and X-ray photoelectron spectroscopy (XPS) further confirmed that NSs are composed of Ti and O, which indicated that the phase composition remains good after exfoliation (Fig. 1L). The TiO NSs were dispersed in PBS, saline, and medium to form a 100 μg mL^{-1} solution. After standing for 48 hours, there was no obvious precipitation in the solution, which suggests that the obtained TiO NSs have good dispersibility (Fig. S2, ESI†).

As a macroscopic black metal oxide semiconductor material, TiO NSs have strong light absorption in the region from ultraviolet to near-infrared, and the absorption intensity decreases with increasing wavelength (Fig. 2A). To study the photothermal conversion performance of TiO NSs dispersions of different concentrations, a near-infrared laser was used to irradiate TiO NSs suspensions of different powers (0.25, 0.5, 1, 1.5, 2.0 W cm^{-2}), which is shown in Fig. 2B–E. The temperature rise of the TiO NSs suspension is positively correlated with the

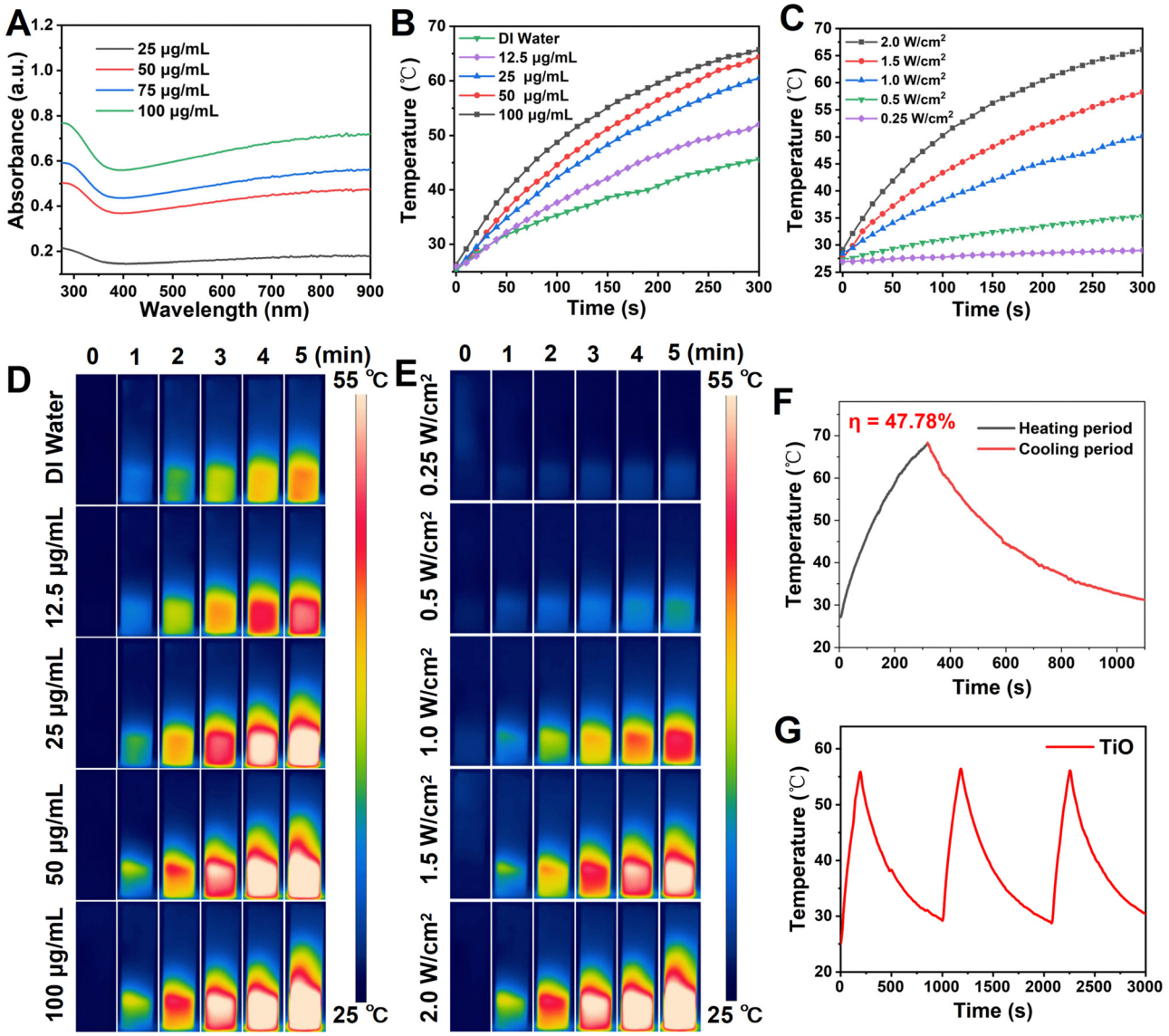

Fig. 2 Characterization of photothermal properties of TiO NSs. (A) The ultraviolet-visible absorption spectra of different concentrations of TiO NSs suspensions. (B) The temperature rise curves of different concentrations of TiO NSs suspensions under infrared light (808 nm, 2.0 W cm^{-2}). (C) Temperature rise curves of 100 μg mL^{-1} TiO NSs suspensions under infrared light with different power densities. (D) Infrared thermography under laser irradiation (2.0 W cm^{-2}). (E) Infrared thermography of TiO NSs suspensions (100 μg mL^{-1}) under infrared light with different power densities (0.25, 0.5, 1.0, 1.5, and 2.0 W cm^{-2}). (F) The temperature rise curve of TiO NSs suspensions (100 μg mL^{-1}) under infrared light and the cooling curve after turning off infrared light. (G) Turning on-off temperature variation of TiO NSs suspensions for three cycles.

NS concentration and laser power. The TiO NSs suspension (100 μg mL^{-1}) reached a temperature of 65 °C under 2.0 W cm^{-2} laser irradiation. Due to excessive protein inactivation and damage to cell membranes, TiO is sufficient for effective short-term high-temperature sterilization. To further evaluate the photothermal properties of the TiO NSs, the conversion efficiency (PTCE) of the TiO NSs was measured by a photothermal method. Based on the sample system time constant τ_s being 313.38 s, 47.78% PTCE can be obtained by fitting the cooling cycle time with the negative natural logarithm of the dynamic temperature.[43,44] The photothermal stability of the TiO NSs was evaluated by the above method (Fig. 2F). During the three cycles of irradiation, the maximum temperature before and after irradiation was basically unchanged, indicating that the TiO NSs have good photothermal stability (Fig. 2G). These data show that TiO NSs are an excellent photothermal material that can be used for short-term and efficient sterilization.

Conventional antibiotics are ineffective against multidrug-resistant bacteria.[45,46] Therefore, broad-spectrum inorganic

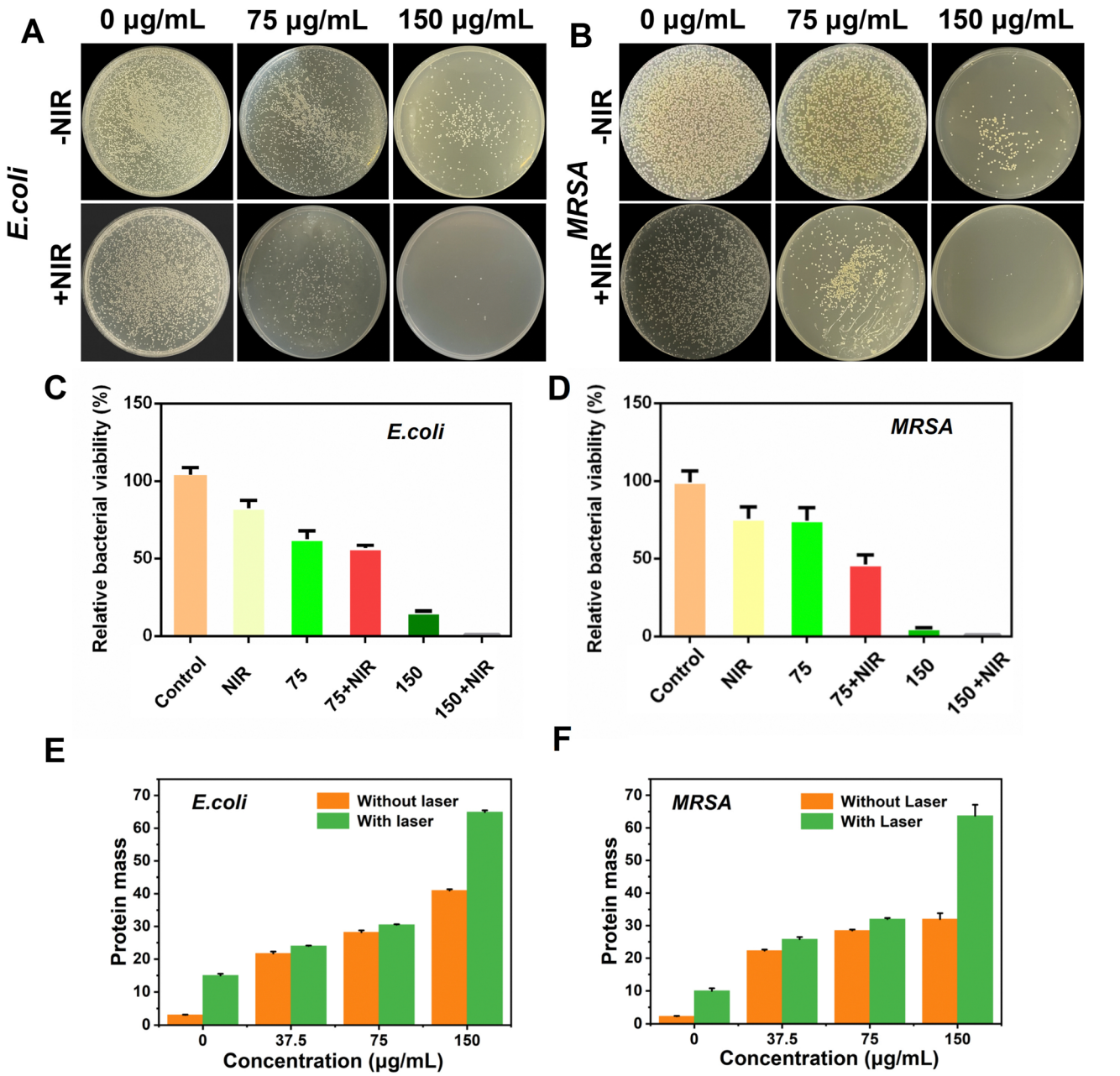

Fig. 3 *In vitro* antibacterial performance test of TiO NSs. (A) Digital photographs of *E. coli* colony formation after different treatments. (B) Digital photographs of *MRSA* colony formation after different treatments. (C) The corresponding relative bacterial activity statistics of *E. coli* in different treatment groups. (D) The corresponding relative bacterial activity statistics of *MRSA* in different treatment groups. Protein leakage statistics of (E) *E. coli* and (F) *MRSA*.

nanomaterial antibacterial agents have attracted increasing attention. Because of TiO's sharp edges and high photothermal properties, we infer that TiO NSs can be used as an effective 2D antimicrobial agent against a wide range of pathogens without fear of resistance. Similarly, *E. coli* and *MRSA* are used as typical models for Gram-negative and Gram-positive bacteria to study the performance of TiO NSs. As shown in Fig. 3A and B, TiO NSs can only partially kill bacteria without laser irradiation. In the presence of 75 μg mL^{-1} TiO NSs, the bacterial activity of *E. coli* and *MRSA* was 65% and 75%, respectively. As the concentration of TiO NSs increases, the bactericidal effect increases. Titanium monoxide is a titanium dioxide with an oxygen vacancy and therefore has similar catalytic properties to titanium dioxide. In sunlight containing ultraviolet light, oxygen in water was converted into superoxide anions by TiO NSs. Superoxide anions also have a certain bactericidal effect. Therefore, the intrinsic antibacterial effect of TiO NSs is due to the synergistic effect of photocatalysis of TiO NSs and the cutting effect of nanosheets. However, even if the concentration of TiO NSs reaches 150 μg mL^{-1}, they cannot completely eliminate *E. coli* and *MRSA*, and the bacterial activity is only 20% and 8%, respectively. The results show that TiO NSs themselves have a good bactericidal effect, and the antibacterial activity of TiO NSs can be greatly improved under NIR light irradiation. After 5 min of irradiation with an 808 nm laser (1.0 W cm^{-2}), the activities of *E. coli* and *MRSA* in the 75 μg mL^{-1} TiO group were 55% and 45%, respectively. The bactericidal effect of TiO NSs was more significant at high concentrations. In particular, the activity of *E. coli* and *MRSA* bacteria was virtually zero after treatment with 150 μg mL^{-1} TiO NSs under near-infrared laser irradiation (1.0 W cm^{-2} for 6 min) (Fig. 3C and D). The amount of protein leakage in different treatment groups was further detected to evaluate the antibacterial effect of TiO NSs. As shown in Fig. 3E and F, TiO NSs had maximum protein leakage at 150 μg mL^{-1} under NIR irradiation. Therefore, we can conclude that TiO NSs kill bacteria by destroying the bacterial membrane and causing the leakage of substances inside the bacteria under NIR light.

To evaluate the antimicrobial properties of TiO NSs, bacterial samples treated using different methods were incubated for 30 min using SYTO 9 and propidium iodide, and then live and dead bacteria were observed under a fluorescence microscope. Live/dead (green/red) bacterial staining (Fig. 4A and B) showed that a very small number of dead cells could be detected under NIR irradiation alone. When treated with TiO NSs alone, the bacteria partially died. However, the fluorescence intensity of the

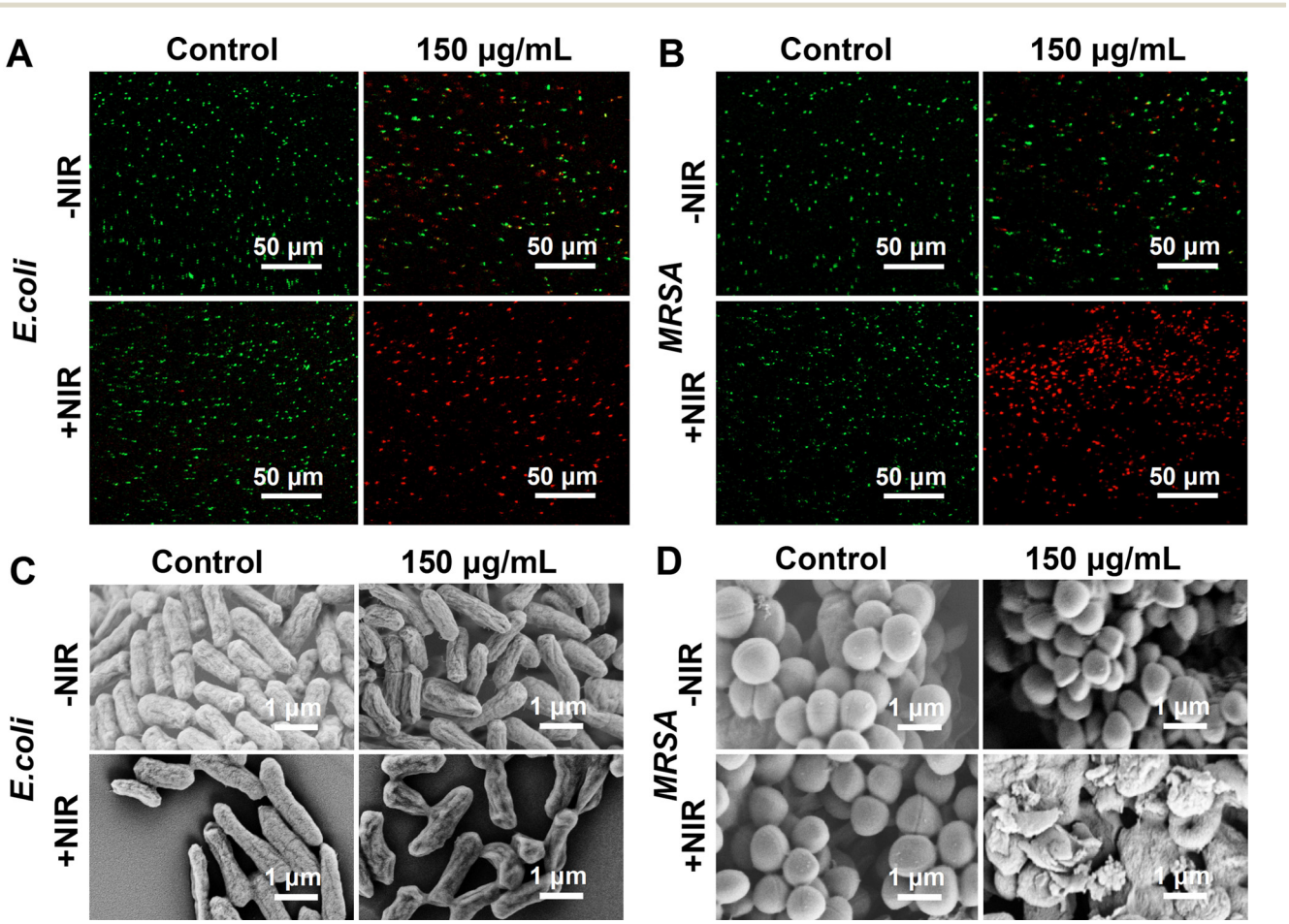

Fig. 4 Characterization of live/dead bacteria. Fluorescence images of live and dead staining of (A) *E. coli* and (B) *MRSA* in different treatment groups. SEM images of (C) *E. coli* and (D) *MRSA* samples in different treatments.

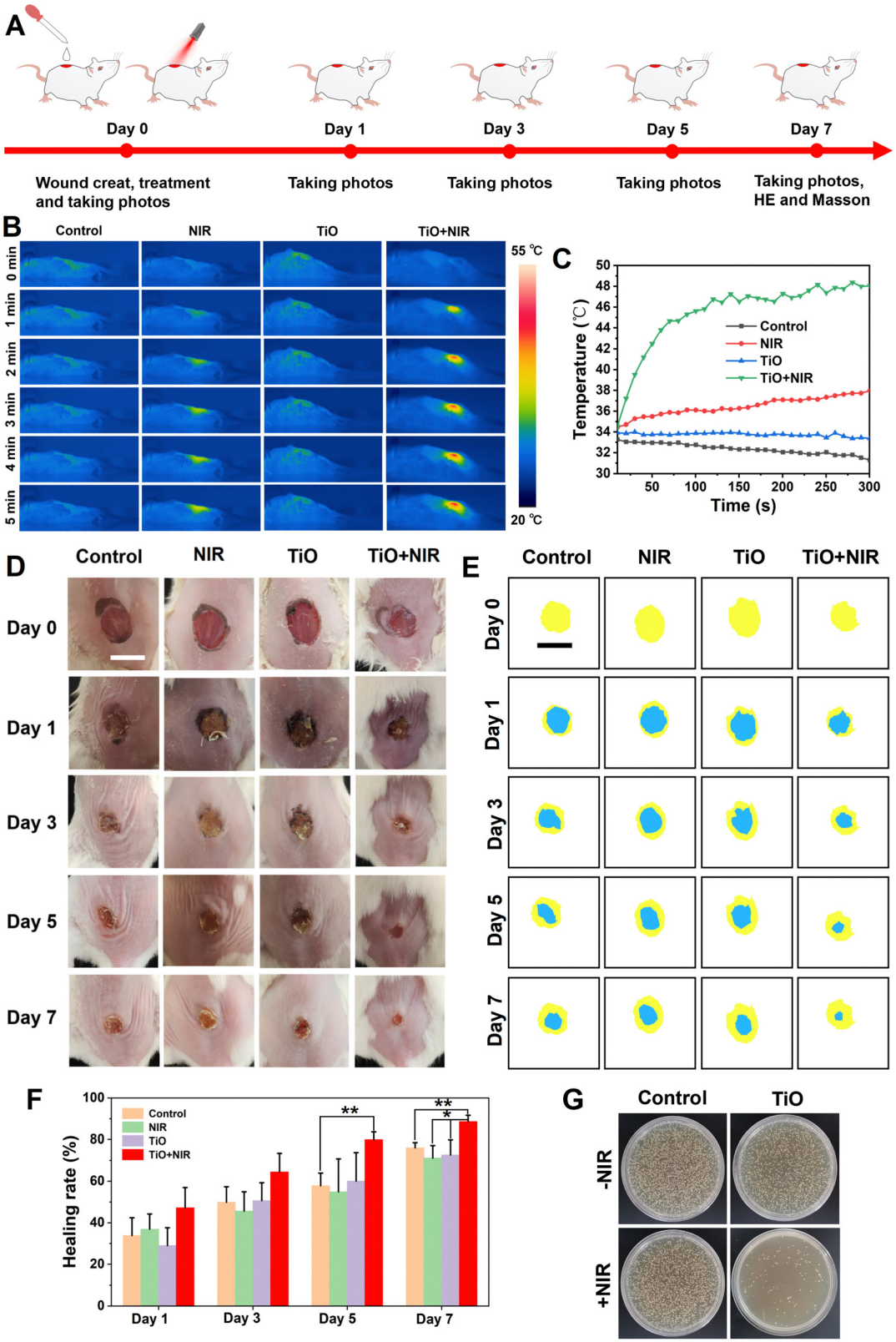

Fig. 5 Therapeutic effects of TiO NSs in promoting infected wound healing. (A) Schematic diagram of the animal experiment process. (B) Thermal imaging images of mice under different treatments (808 nm, 1.0 W cm^{-2}, 5 min). (C) Corresponding changes in wound maximum temperature. (D) Digital photos of wounds in different treatment groups on days 0, 1, 3, 5, and 7. The scale bar is 1 cm. (E) Changes in wound area from day 1 to day 7. (F) Wound healing rate data statistics in the control, NIR, TiO, and TiO groups (*$P < 0.05$, **$P < 0.01$). (G) The statistical data of MRSA colonies in the skin wound on Day 7.

TiO group under near-infrared irradiation was completely red, indicating that the bacteria in the TiO NSs group died completely under near-infrared irradiation, which was very consistent with the results of the spread plate experiment. After NIR light irradiation, the morphology of bacteria in each group was observed by scanning electron microscopy. The TiO NSs group had the most serious morphological deformation (Fig. 4C and D). Some *MRSA* cells are morphologically impaired, possibly due in part to membrane damage caused by sharp edges of TiO NSs. The nanosheet structure is thought to cut and damage cell membranes, causing contents to leak out. The morphology of bacteria in the control groups remained good. In the TiO NSs group, the bacteria contracted slightly. These results suggested that the structures and functions of bacteria were more vulnerable to damage at high temperatures.

The *in vivo* antibacterial potential of TiO was evaluated using a mouse bacterial infection model, and the treatment strategies are shown in Fig. 5A. The photothermal properties of the TiO suspension *in vivo* were evaluated by an infrared camera after it was dropped into the wound surface of the back of rats. As shown in Fig. 5B and C, after 5 min of NIR irradiation at 808 nm (W cm^{-2}), the temperature of the wound area

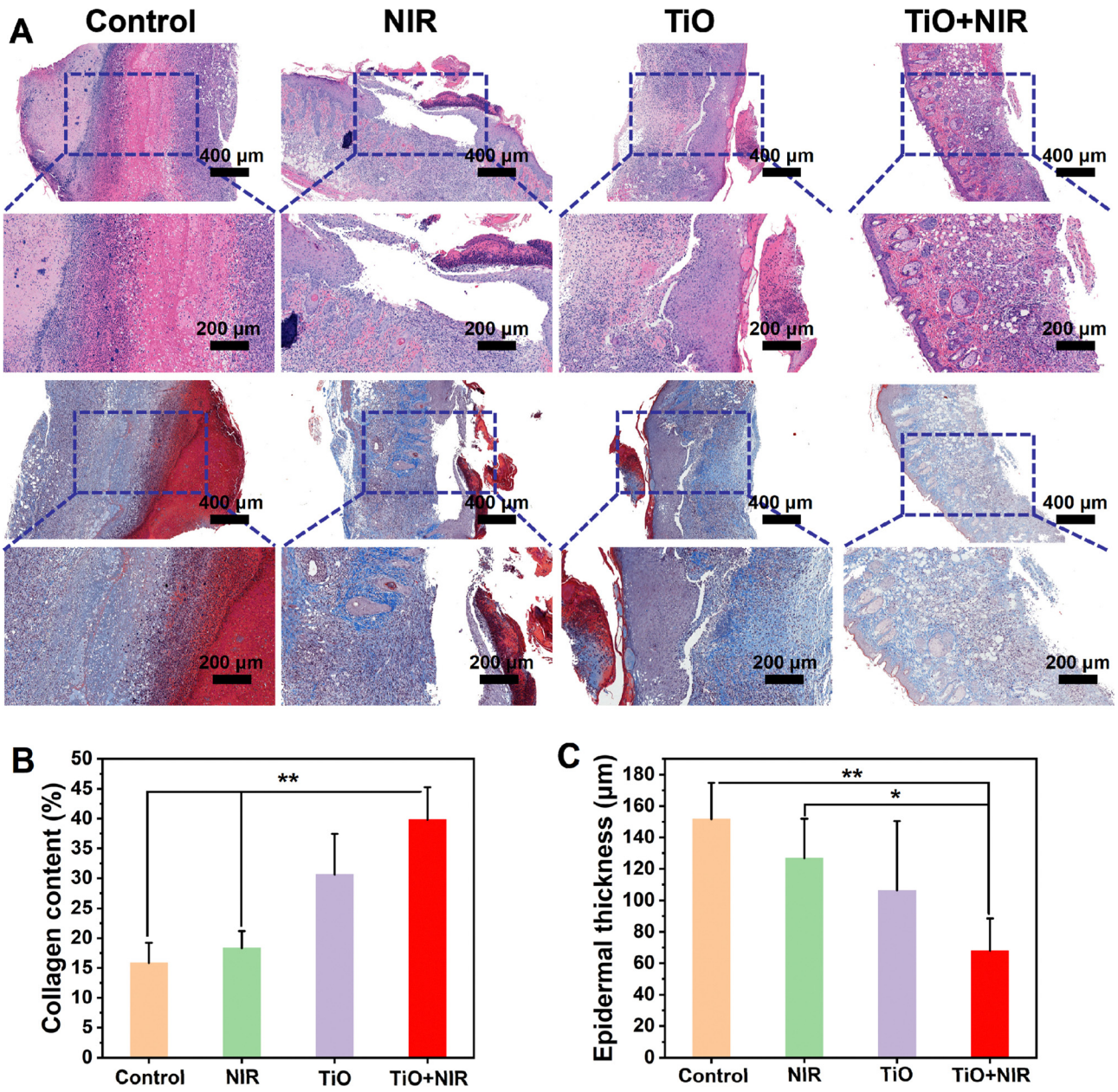

Fig. 6 Statistics of collagen deposition and epithelial thickness. (A) H&E and Masson staining of skin tissue in the control, NIR, TiO, and TiO + NIR groups on day 7. (B) The collagen content and (C) Epidermal thickness of each group 7 days after the treatment, detected by H&E and Masson staining of skin tissue (*$P < 0.05$, **$P < 0.01$).

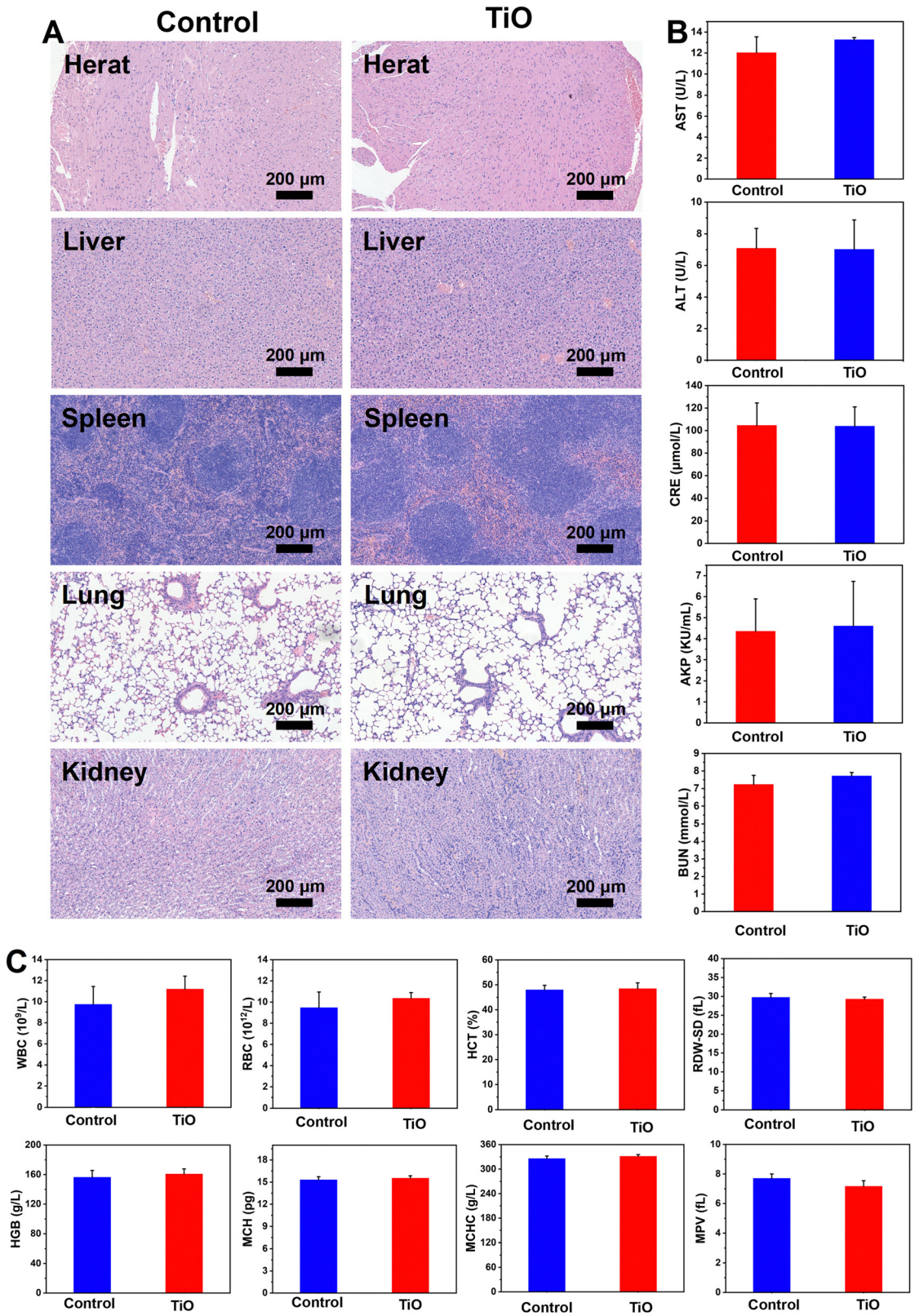

Fig. 7 Biosafety evaluation of TiO NSs. (A) H&E staining of major organ tissues of experimental mice in the control and TiO groups. The scale bar is 100 μm. (B) Blood routine and (C) Biochemical levels after different treatments.

covered by TiO rose to 45 °C, while the temperature of the wound area not covered by TiO rose to only 38 °C under the same conditions. The healing information of wounds at different time points is presented in Fig. 5D–F. On the 7th day,

the wound area in the TIO + NIR group was much smaller than that in the other groups. On day 7, the wound healing rate in the TiO + NIR group was 88.6%, while those in the control group, NIR group, and TiO group were 76.1%, 71.2%, and 72.7%, respectively. These results indicate that the wound healing effect of the TiO + NIR group is better than that of the other groups. On the 7th day, the agar plate approach was used to detect the number of bacteria in the wound area of each treatment group and evaluate its bactericidal effect. The control group had a large number of bacteria on the agar plate, while the TiO + NIR group had a small number of bacteria on the agar plate. These results intuitively suggested that TiO had great promise as an antimicrobial agent.

To further evaluate the healing quality of the skin tissues in the four groups, hematoxylin and eosin staining (H&E) and Masson staining were performed on the 7th day. H&E staining results showed that the dermis of the control group and the NIR group were seriously damaged and that the epithelial tissue was discontinuous (Fig. 6A). At the same time, continuous thick epithelial tissue formed at the wound site in the TiO group. In the TiO + NIR group, the thickness of epithelial tissue was significantly reduced, similar to that of normal skin tissue. The key to skin tissue regeneration during wound healing is the formation of epithelial tissue and collagen. H&E staining was used to calculate epithelial tissue thickness in each group, and the results are shown in Fig. 6B. The collagen content in each group was quantitatively analyzed by Masson trichromatic staining (Fig. 6C). The collagen content in the TiO + NIR group ($39.9 \pm 5.4\%$) was much higher than that in the TiO group ($30.6 \pm 6.8\%$) and other groups ($15.9 \pm 3.4\%$ and $18.3 \pm 2.9\%$). These results further support TiO + NIR as a treatment strategy to accelerate the skin wound healing process by killing bacteria and promoting skin wound epithelial formation and collagen deposition.

On the 7th day after wound treatment, H&E staining was performed on the major organs of each group to evaluate their biocompatibility and biosafety. As shown in Fig. 7A, no obvious inflammatory cell infiltration or injury was observed in the major organs (heart, liver, spleen, lung, and kidney). The contents of liver-, kidney- and blood-related markers were further detected by routine blood and biochemical examinations. There were no significant changes in blood biochemical indicators (AST, ALT, CRE, AKP, BUN) or routine liver indicators (WBC, RBC, HCT, RDW-SD, HGB, MCH, MCHC, MPV) in all treatment groups, which were all within the normal range (Fig. 7B and C). These results showed that TiO NSs did not cause acute toxicity and did not damage the liver and kidney functions of mice. Hemolysis was also assessed to explore biocompatibility. The TiO NSs did not induce obvious hemolysis even at a concentration of 200 μg mL^{-1} (Fig. S3, ESI†). Cell experiments showed that TiO NSs had no obvious cytotoxicity when the concentration of TiO NSs reached 100 μg mL^{-1} (Fig. S4, ESI†). Above all, TiO NSs have good biological safety and great potential for clinical application.

Conclusions

We successfully prepared 2D TiO NSs and demonstrated that TiO NSs can be used as high-performance antibacterial agents to promote wound healing. TiO NSs can be produced in large quantities by an ultrasonic-assisted liquid-phase exfoliation method. Acquired TiO NSs have intrinsic antimicrobial properties, possibly due to membrane damage caused by sharp edges. In addition, TiO NSs have a strong near-infrared light absorption capacity and higher PTCE, which can effectively sterilize bacteria under near-infrared light irradiation. Because of these two antibacterial mechanisms, *E. coli* and *MRSA* can be effectively killed. In particular, these two bacteria were completely destroyed after treatment with low concentrations of TiO + NIR light for six minutes. Animal experiments further confirmed its good bacterial characteristics *in vivo*. TiO NSs have no significant toxic side effects, indicating a high potential for biomedical applications. Therefore, TiO NSs are promising broad-spectrum antimicrobial nanoagents that can be applied to a wide range of pathogenic bacteria, especially multidrug-resistant bacteria.

Conflicts of interest

The authors declare no competing financial interest.

Acknowledgements

This work was supported by the National Natural Science Foundation of China (No. 52202343), Anhui Provincial Natural Science Foundation (2208085QC81), Basic and Clinical Cooperative Research and Promotion Program of Anhui Medical University (2021xkjT028), Research Fund of Anhui Institute of Translational Medicine (2022zhyx-C01), the Youth Research Project of Chinese Nursing Association (ZHKYQ202213), Postdoctoral Research Activities in Anhui Province (2022B583), Scientific Research Project of Colleges and Universities in Anhui Province (2022AH050744), and National Innovative Training Program for College Students (202210366007). The authors would like to thank the Shiyanjia lab (**www.shiyanjia.com**) for their help in language polishing.

References

1 X. Zhou, Z. Wang, Y. K. Chan, Y. Yang, Z. Jiao, L. Li, J. Li, K. Liang and Y. Deng, Infection micromilieu-activated nanocatalytic membrane for orchestrating rapid sterilization and stalled chronic wound regeneration, *Adv. Funct. Mater.*, 2022, **32**(7), 2109469.

2 X. Chu, Y. Liu, P. Zhang, K. Li, W. Feng, B. Sun, N. Zhou and J. Shen, Silica-supported near-infrared carbon dots and bicarbonate nanoplatform for triple synergistic sterilization and wound healing promotion therapy, *J. Colloid Interface Sci.*, 2022, **608**, 1308–1322.

3 L. Liu, J. Shi, X. Sun, Y. Zhang, J. Qin, S. Peng, J. Xu, L. Song and Y. Zhang, Thermo-responsive hydrogel-supported antibacterial

material with persistent photocatalytic activity for continuous sterilization and wound healing, *Composites, Part B*, 2022, **229**, 109459.

4 S. Hui, Q. Liu, Y. Han, L. Zhang, J. Yang, S. Jiang, H. Qian and W. Yang, ICG@ ZIF-8/PDA/Ag composites as chemo-photothermal antibacterial agents for efficient sterilization and enhanced wound disinfection, *J. Mater. Chem. B*, 2021, **9**(48), 9961–9970.

5 F. Gao, T. Shao, Y. Yu, Y. Xiong and L. Yang, Surface-bound reactive oxygen species generating nanozymes for selective antibacterial action, *Nat. Commun.*, 2021, **12**(1), 745.

6 X. Wang, L. Fan, L. Cheng, Y. Sun, X. Wang, X. Zhong, Q. Shi, F. Gong, Y. Yang and Y. Ma, Biodegradable nickel disulfide nanozymes with GSH-depleting function for high-efficiency photothermal-catalytic antibacterial therapy, *iscience*, 2020, **23**(7), 101281.

7 C. Chakansin, J. Yostaworakul, C. Warin, K. Kulthong and S. Boonrungsiman, Resazurin rapid screening for antibacterial activities of organic and inorganic nanoparticles: Potential, limitations and precautions, *Anal. Biochem.*, 2022, **637**, 114449.

8 R. R. Choudhury, J. M. Gohil, S. Mohanty and S. K. Nayak, Antifouling, fouling release and antimicrobial materials for surface modification of reverse osmosis and nanofiltration membranes, *J. Mater. Chem. A*, 2018, **6**(2), 313–333.

9 V. M. Wu, S. Tang and V. Uskokovic, Calcium phosphate nanoparticles as intrinsic inorganic antimicrobials: the antibacterial effect, *ACS Appl. Mater. Interfaces*, 2018, **10**(40), 34013–34028.

10 S. Saidin, M. A. Jumat, N. A. A. M. Amin and A. S. S. Al-Hammadi, Organic and inorganic antibacterial approaches in combating bacterial infection for biomedical application, *Mater. Sci. Eng., C*, 2021, **118**, 111382.

11 R. Dastjerdi and M. Montazer, A review on the application of inorganic nano-structured materials in the modification of textiles: focus on anti-microbial properties, *Colloids Surf., B*, 2010, **79**(1), 5–18.

12 F. Wei, X. Cui, Z. Wang, C. Dong, J. Li and X. Han, Recoverable peroxidase-like Fe_3O_4@ MoS_2-Ag nanozyme with enhanced antibacterial ability, *Chem. Eng. J.*, 2021, **408**, 127240.

13 Z. Qin, Y. Zheng, Y. Wang, T. Du, C. Li, X. Wang and H. Jiang, Versatile roles of silver in Ag-based nanoalloys for antibacterial applications, *Coord. Chem. Rev.*, 2021, **449**, 214218.

14 W. Luo, B. Hu, H.-L. Zhang, C. Li, Y. Shi, X. Li and L. Jin, Antibacterial, photothermal and stable Ag-titanium-oxo-clusters hydrogel designed for wound healing, *Mater. Des.*, 2023, **226**, 111674.

15 M. L. Ermini and V. Voliani, Antimicrobial nano-agents: the copper age, *ACS Nano*, 2021, **15**(4), 6008–6029.

16 D. Mitra, E.-T. Kang and K. G. Neoh, Antimicrobial copper-based materials and coatings: potential multifaceted biomedical applications, *ACS Appl. Mater. Interfaces*, 2019, **12**(19), 21159–21182.

17 K. Wu, D. Zhu, X. Dai, W. Wang, X. Zhong, Z. Fang, C. Peng, X. Wei, H. Qian and X. Chen, Bimetallic oxide $Cu_{1.5}Mn_{1.5}O_4$ cage-like frame nanospheres with triple enzyme-like activities for bacterial-infected wound therapy, *Nano Today*, 2022, **43**, 101380.

18 X. Wang, Q. Shi, Z. Zha, D. Zhu, L. Zheng, L. Shi, X. Wei, L. Lian, K. Wu and L. Cheng, Copper single-atom catalysts with photothermal performance and enhanced nanozyme activity for bacteria-infected wound therapy, *Bioact. Mater.*, 2021, **6**(12), 4389–4401.

19 S. N. Riduan and Y. Zhang, Recent Advances of Zinc-based Antimicrobial Materials, *Chem. – Asian J.*, 2021, **16**(18), 2588–2595.

20 G. Prado-Prone, P. Silva-Bermudez, A. Almaguer-Flores, J. A. García-Macedo, V. I. García, S. E. Rodil, C. Ibarra and C. Velasquillo, Enhanced antibacterial nanocomposite mats by coaxial electrospinning of polycaprolactone fibers loaded with Zn-based nanoparticles, *Nanomedicine*, 2018, **14**(5), 1695–1706.

21 W. Liang, J. Cheng, J. Zhang, Q. Xiong, M. Jin and J. Zhao, pH-Responsive on-demand alkaloids release from core–shell ZnO@ZIF-8 nanosphere for synergistic control of bacterial wilt disease, *ACS Nano*, 2022, **16**(2), 2762–2773.

22 A. F. Halbus, T. S. Horozov and V. N. Paunov, Strongly enhanced antibacterial action of copper oxide nanoparticles with boronic acid surface functionality, *ACS Appl. Mater. Interfaces*, 2019, **11**(13), 12232–12243.

23 S. Kaul, P. Sagar, R. Gupta, P. Garg, N. Priyadarshi and N. K. Singhal, Mechanobactericidal, gold nanostar hydrogel-based bandage for bacteria-infected skin wound healing, *ACS Appl. Mater. Interfaces*, 2022, **14**(39), 44084–44097.

24 Y. Tu, M. Lv, P. Xiu, T. Huynh, M. Zhang, M. Castelli, Z. Liu, Q. Huang, C. Fan and H. Fang, Destructive extraction of phospholipids from Escherichia coli membranes by graphene nanosheets, *Nat. Nanotechnol.*, 2013, **8**(8), 594–601.

25 Z. Miao, L. Fan, X. Xie, Y. Ma, J. Xue, T. He and Z. Zha, Liquid exfoliation of atomically thin antimony selenide as an efficient two-dimensional antibacterial nanoagent, *ACS Appl. Mater. Interfaces*, 2019, **11**(30), 26664–26673.

26 S. Pandit, S. Karunakaran, S. K. Boda, B. Basu and M. De, High antibacterial activity of functionalized chemically exfoliated MoS_2, *ACS Appl. Mater. Interfaces*, 2016, **8**(46), 31567–31573.

27 A. Sethulekshmi, A. Saritha, K. Joseph, A. S. Aprem and S. B. Sisupal, MoS_2 based nanomaterials: Advanced antibacterial agents for future, *J. Controlled Release*, 2022, **348**, 158–185.

28 Z. Sun, Y. Zhang, H. Yu, C. Yan, Y. Liu, S. Hong, H. Tao, A. W. Robertson, Z. Wang and A. A. Pádua, New solvent-stabilized few-layer black phosphorus for antibacterial applications, *Nanoscale*, 2018, **10**(26), 12543–12553.

29 D. Zhang, H. M. Liu, X. Shu, J. Feng, P. Yang, P. Dong, X. Xie and Q. Shi, Nanocopper-loaded Black phosphorus nanocomposites for efficient synergistic antibacterial application, *J. Hazard. Mater.*, 2020, **393**, 122317.

30 S. Liu, X. Pan and H. Liu, Two-dimensional nanomaterials for photothermal therapy, *Angew. Chem.*, 2020, **132**(15), 5943–5953.

31 Y. Chen, Y. Gao, Y. Chen, L. Liu, A. Mo and Q. Peng, Nanomaterials-based photothermal therapy and its potentials in antibacterial treatment, *J. Controlled Release*, 2020, **328**, 251–262.

32 H. Hu, H. Wang, Y. Yang, J. F. Xu and X. Zhang, A Bacteria-Responsive Porphyrin for Adaptable Photodynamic/Photothermal Therapy, *Angew. Chem.*, 2022, **134**(23), e202200799.

33 B. Hu, C. Berkey, T. Feliciano, X. Chen, Z. Li, C. Chen, S. Amini, M. H. Nai, Q. L. Lei and R. Ni, Thermal-Disrupting Interface Mitigates Intercellular Cohesion Loss for Accurate Topical Antibacterial Therapy., *Adv. Mater.*, 2020, **32**(12), 1907030.

34 Y. Liu, Z. Guo, F. Li, Y. Xiao, Y. Zhang, T. Bu, P. Jia, T. Zhe and L. Wang, Multifunctional magnetic copper ferrite nanoparticles as Fenton-like reaction and near-infrared photothermal agents for synergetic antibacterial therapy, *ACS Appl. Mater. Interfaces*, 2019, **11**(35), 31649–31660.

35 Y. Gao, Y. Dong, S. Yang, A. Mo, X. Zeng, Q. Chen and Q. Peng, Size-dependent photothermal antibacterial activity of $Ti_3C_2T_x$ MXene nanosheets against methicillin-resistant Staphylococcus aureus, *J. Colloid Interface Sci.*, 2022, **617**, 533–541.

36 S. Zhang, Q. Lu, F. Wang, Z. Xiao, L. He, D. He and L. Deng, Gold–platinum nanodots with high-peroxidase-like activity and photothermal conversion efficiency for antibacterial therapy, *ACS Appl. Mater. Interfaces*, 2021, **13**(31), 37535–37544.

37 S. Yu, G. Li, P. Zhao, Q. Cheng, Q. He, D. Ma and W. Xue, NIR-laser-controlled hydrogen-releasing PdH nanohydride for synergistic hydrogen-photothermal antibacterial and wound-healing therapies, *Adv. Funct. Mater.*, 2019, **29**(50), 1905697.

38 S. Amano, D. Bogdanovski, H. Yamane, M. Terauchi and R. Dronskowski, ε-TiO, a Novel Stable Polymorph of Titanium Monoxide, *Angew. Chem.*, 2016, **128**(5), 1684–1689.

39 J. Xu, D. Wang, H. Yao, K. Bu, J. Pan, J. He, F. Xu, Z. Hong, X. Chen and F. Huang, Nano titanium monoxide crystals and unusual superconductivity at 11 K, *Adv. Mater.*, 2018, **30**(10), 1706240.

40 X. Wang, X. Zhong, L. Bai, J. Xu, F. Gong, Z. Dong, Z. Yang, Z. Zeng, Z. Liu and L. Cheng, Ultrafine titanium monoxide (TiO_{1+x}) nanorods for enhanced sonodynamic therapy, *J. Am. Chem. Soc.*, 2020, **142**(14), 6527–6537.

41 X. Wang, X. Zhong and L. Cheng, Titanium-based nanomaterials for cancer theranostics, *Coord. Chem. Rev.*, 2021, **430**, 213662.

42 X. Wang, X. Wang, Q. Yue, H. Xu, X. Zhong, L. Sun, G. Li, Y. Gong, N. Yang and Z. Wang, Liquid exfoliation of TiN nanodots as novel sonosensitizers for photothermal-enhanced sonodynamic therapy against cancer, *Nano Today*, 2021, **39**, 101170.

43 Y. Ma, K. Jiang, H. Chen, Q. Shi, H. Liu, X. Zhong, H. Qian, X. Chen, L. Cheng and X. Wang, Liquid exfoliation of V_8C_7 nanodots as peroxidase-like nanozymes for photothermal-catalytic synergistic antibacterial treatment, *Acta Biomater.*, 2022, **149**, 359–372.

44 D. Liu, X. Dai, W. Zhang, X. Zhu, Z. Zha, H. Qian, L. Cheng and X. Wang, Liquid exfoliation of ultrasmall zirconium carbide nanodots as a noninflammatory photothermal agent in the treatment of glioma, *Biomaterials*, 2023, **292**, 121917.

45 W. Sun and F. G. Wu, Two-Dimensional Materials for Antimicrobial Applications: Graphene Materials and Beyond, *Chem. - Asian J.*, 2018, **13**(22), 3378–3410.

46 G. Gao, Y. W. Jiang, H. R. Jia and F. G. Wu, Near-infrared light-controllable on-demand antibiotics release using thermo-sensitive hydrogel-based drug reservoir for combating bacterial infection, *Biomaterials*, 2019, **188**, 83–95.